Insect Flight: From Newton's Law to Neurons

Z. Jane Wang[1,2]

[1]Department of Physics, Cornell University, Ithaca, New York 14853;
email: jane.wang@cornell.edu

[2]Sibley School of Mechanical and Aerospace Engineering, Cornell University, Ithaca,
New York 14853

Keywords

physics of behavior, animal locomotion, aerodynamics, flight stability and
control, flight reflex, neural feedback control, halteres, motor neurons,
steering muscles

Abstract

Why do animals move the way they do? Bacteria, insects, birds, and fish
share with us the necessity to move so as to live. Although each organism
follows its own evolutionary course, it also obeys a set of common laws. At
the very least, the movement of animals, like that of planets, is governed
by Newton's law: All things fall. On Earth, most things fall in air or water,
and their motions are thus subject to the laws of hydrodynamics. Through
trial and error, animals have found ways to interact with fluid so they can
float, drift, swim, sail, glide, soar, and fly. This elementary struggle to escape
the fate of falling shapes the development of motors, sensors, and mind.
Perhaps we can deduce parts of their neural computations by understanding
what animals must do so as not to fall. Here I discuss recent developments
along this line of inquiry in the case of insect flight. Asking how often a fly
must sense its orientation in order to balance in air has shed new light on the
role of motor neurons and steering muscles responsible for flight stability.

1. INTRODUCTION

1.1. Motivation

Why do animals move the way they do? Bacteria, insects, birds, and fish share with us the necessity to move so as to live. Although each organism follows its own evolutionary course, it also obeys a set of common laws. At the very least, the movement of animals, like that of planets, is governed by Newton's law: All things fall. On Earth, most things fall in air or water, and their motions are thus subject to the laws of hydrodynamics. Through trial and error, animals have found ways to interact with fluid so they can float, drift, swim, sail, glide, soar, and fly. This elementary struggle to escape the fate of falling shapes the development of motors, sensors, and mind. Perhaps we can deduce parts of their neural computations by understanding what animals must do so as not to fall. Here I review recent developments along this line of inquiry in the case of insect flight. Asking how often a fly must sense its orientation in order to balance in air has shed new light on the role of the first basalar muscle, one of the fly's steering muscles, in regulating flight stability (1).
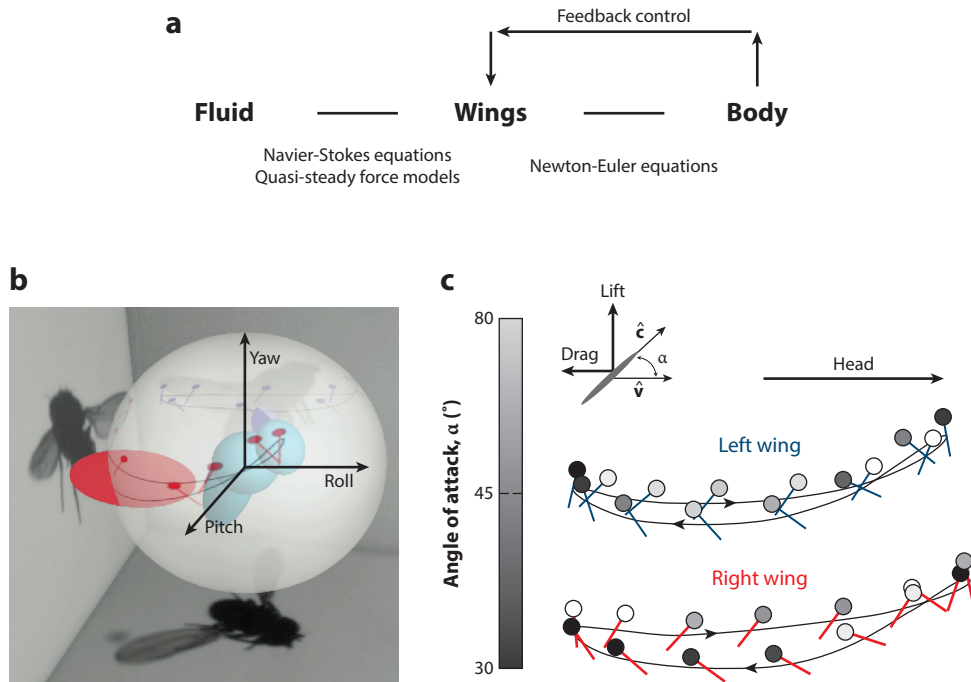
1.2. Laws of Movement and Neural Computations

Living life on wings, insects carry out a wide variety of neural computations "on the fly" in tens of milliseconds. They sense their own state while moving and must separate the movement of the external world from their own. Moreover, they respond to almost all external stimuli by adjusting their wing motion. Their algorithms for actions therefore must take into account the laws of movement. The two macroscopic laws governing flight are the Navier-Stokes equations for the wing and flow interactions and the Newton-Euler equations for the dynamic coupling between the body and the wings (**Figure 1**). These equations are responsible for the aerodynamic forces on the flapping wings and the consequent motion and stability of the body. Understanding how these physical laws have shaped insects' internal computations is critical to mechanistic explanations of animals' behavior.

2. STABILITY OF FLAPPING FLIGHT

One place where we find a connection between flight dynamics and the design of neural circuitry is in insects' balancing acts. To balance in air, insects need to not only generate enough force but also make small adjustments in wing motion to remain stable. Without neural feedback control, their flight is unstable, similar to our standing posture. Such instability may seem inconvenient, as it requires constant microadjustments to stand upright, but it does make walking easier. All we need to do is to lean forward and catch ourselves (3). Perhaps for the same reason, insects choose to fly at the boundary between stability and instability.

2.1. Time-Averaged Dynamic Model

The cause of instability in flapping flight is different from that in fixed-wing flight (4, 5). To get some intuition about the nature of instability, we can analyze flight stability in the limit where the wing flaps at a much faster rate than the oscillation of the body. In such a limit, it is reasonable to average the aerodynamic forces over a wing period to simplify the dynamic equations for flapping flight. Taking the motion along a longitudinal plane as an example, the body dynamic state is given by a set of four independent variables, the two translational velocities along the symmetric plane, (U_x, U_z), and the body pitch orientation and pitching rate (θ_b, ω_b) (**Figure 2a**). The dynamics are given by Newton's law in the presence of aerodynamic forces. The governing equations, expressed

a

Feedback control

Fluid ——— **Wings** ——— **Body**

Navier-Stokes equations
Quasi-steady force models

Newton-Euler equations

b

c

Figure 1

(*a*) The key components in models of insect flight. (*b*) Naming convention for body rotation. Pitch and roll axes are defined in the mean stroke plane. (*c*) Wing motion during a saccade, a rapid yaw rotation, viewed from the side (2).

in the comoving coordinates with body, (x', z'), are

$$m\dot{U}_{x'} = \omega U_{z'} + \langle F_{x'} \rangle \sin\theta + g\sin\theta, \qquad 1.$$

$$m\dot{U}_{z'} = -\omega U_{x'} + \langle F_{z'} \rangle \cos\theta - g\cos\theta, \qquad 2.$$

$$I\dot{\omega} = -\langle F_{x'} \rangle b, \qquad 3.$$

$$\dot{\theta} = \omega, \qquad 4.$$

where $\langle F_{x',z'} \rangle$ represent the aerodynamic lift, F_L, and drag, F_D, averaged over a flapping period, decomposed in the body frame. In this model, the wing mass is assumed to be negligible, and thus the inertial coupling between the wing and the body is ignored. The lift and drag depend on the superposition of the body and wing velocities, $\vec{u} = \vec{U} + \vec{U}_W$. In the simplest form of a quasi-steady approximation of the aerodynamic force, the lift and drag are quadratic in velocity, with coefficients depending on the angle of attack, α: $F_{L,D} = \frac{1}{2}\rho C_{L,D}(\alpha)u^2$. For a symmetric plate undergoing a translational motion at intermediate Reynolds numbers, the lift and drag coefficients can be approximated by

$$C_L(\alpha) = C_L(\pi/4)\sin 2\alpha, \qquad 5.$$

$$C_D(\alpha) = C_{D0} + C_D(\pi/2)(1 - \cos 2\alpha). \qquad 6.$$
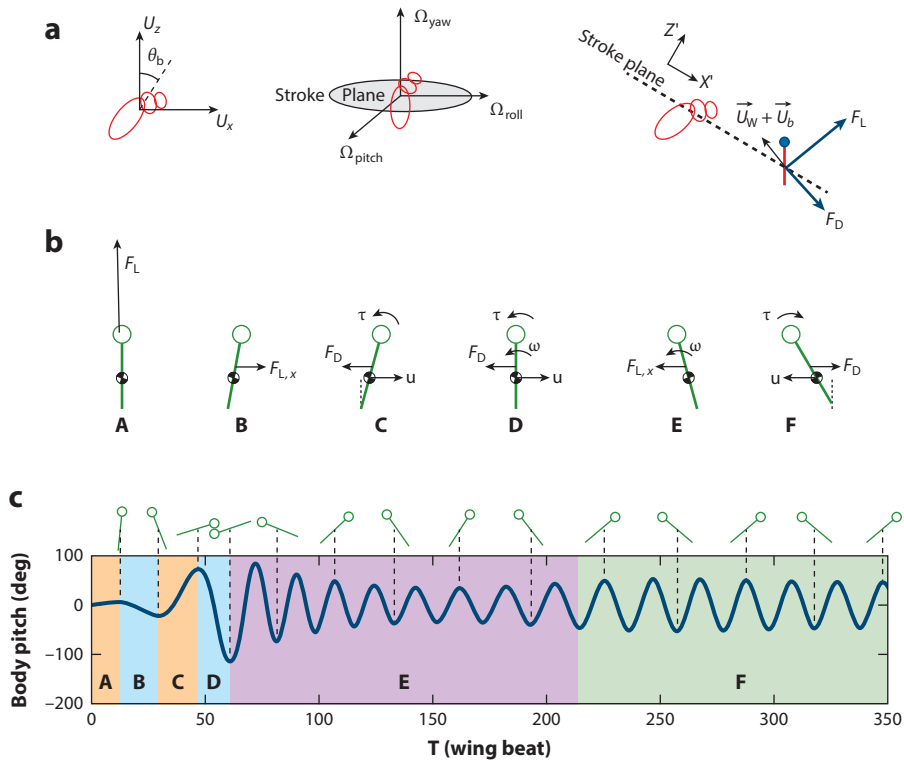
Figure 2

Dynamic instability of a hovering insect. (*a*) (*Left*) The kinematic state of the body in a longitudinal flight is defined by four variables, the two translational velocities, (U_x, U_z), and the pitch orientation and the pitching rate, (θ_b, ω_b). (*Middle*) the body rotation, roll, yaw, and pitch defined in the body coordinates. The pitch and roll axes are in the mean stroke plane. (*Right*) The wing motion in the averaged dynamic model. The wing flaps along a mean stroke plane, with its net velocity given by the sum of the wing and body velocities. Aerodynamic lift, F_L, is normal to the net wing velocity, and aerodynamic drag, F_D, is antiparallel to the velocity. (*b*) The schematics for the onset of pitching instability due to the coupling between the rotation and translational motion. (*c*) Simulation of flapping flight shows the timescale associated with the pitching instability and the steady-state dynamics (1).

They are extracted from the computational and experimental studies of a flapping wing and approximate the forces over a full range of angles of attack during dynamic stall (6), beyond the small angle limit assumed by the Kutta-Joukowski theory. The dependence on 2α reflects the symmetry of a plate, since $\sin 2(\alpha + \pi) = \sin 2\alpha$. In the small angle limit, $\sin 2\alpha \approx 2 \sin \alpha$, and therefore is consistent with the Kutta-Joukowski lift, $C_L(\alpha) = 2\pi \sin \alpha$ (7).

To quantify the stability of flapping flight, recent work has carried out linear stability analyses of averaged dynamic models for longitudinal and lateral flight with various approximations of aerodynamic forces (1, 8–14; for a review, see Reference 15). Flight stability is determined by the largest eigenvalue from the linear stability calculation about an equilibrium, either hovering or a steady state flight. Those that have been studied so far, including hoverflies, bumblebees, fruit flies, locusts, and hawkmoths, all have an unstable mode in hovering, corresponding to the pitch and roll instability.

Although the details differ, the pitch and roll instabilities are caused by a similar mechanism. Both arise from the coupling between the translational and rotational motions. Imagine that a

hovering insect is like a small helicopter, with a spinning disk around its shoulders (**Figure 2a**). The aerodynamic force acts roughly perpendicular to the disk. If we tilt the disk slightly, the body drifts. The drift velocity would modify the aerodynamic force and torque on the body, changing its velocity, which in turn would affect the aerodynamic force. The resulting imbalance in the drag force would introduce a torque that rotates the body, leading to pitch and roll instability (**Figure 2b**). The pitch and roll correspond to the tilt about the two orthogonal axes in the stroke plane (**Figure 2a**).

If the disk were rotated about the axis normal to the plane, the yaw axis, the coupling between the wing and body motions would induce a drag, damping the yaw turn (2, 16–19). This linear damping is not due to air viscosity but due to a generic effect resulting from the dynamic coupling between the body motion and a pair of symmetric wing motions: $\delta F_D = F_D(U_w - \delta U_b) - F_D(U_w + \delta U_b) = -\beta \delta U_b + O(\delta U_b^2)$. The linear damping is present as long as the drag increases with velocity. Because this damping term is absent in tethered flight, the timescales in the dynamics of saccades, a fast yaw rotation, are different during tethered versus free flight (17, 18, 20, 21). The fly takes advantage of this passive damping to simplify its control of yaw rotation. It waits until the body damps its rotation before applying an active torque with asymmetric wing strokes; therefore, it can correct its orientation with a linear controller (19).

2.2. Fully Coupled Dynamics

A subtler effect of flight stability is the timescale over which the instability occurs and the coupling among different degrees of freedom (1). The dynamic timescales for stability affect the timescales of the feedback control used by different insects (9). To analyze this, we need to examine the fully coupled dynamic equations, where the instantaneous coupling between the wing and body motions are included (Section 3). Simulation of free flight illustrates the onset of the pitch instability (**Figure 2b** and **Video 1**) (1). In the first ten wingbeats, the aerodynamic torque pitches the body nose-down (A → B). Thus, the aerodynamic lift tilts forward and drives the insect forward (B → C). The forward motion then couples with the back-and-forth wing motion resulting in a drag that pitches the body up (C → D). The drag and the horizontal component of the lift decelerate the body, and the body eventually moves backward (D → E). The backward motion is coupled with the wing motion to produce a nose-down torque (E → F). The body oscillates as a result of this coupling between the horizontal and body-pitch motions, with a period of ∼20 wingbeats. Because of the oscillation of the body, the weight balance requires a significant descent velocity to induce a vertical drag force. After a transient period, the body reaches a steady descent with a terminal speed of ∼50 cm/s. This transition from an initially unstable hovering state to the final descending periodic state is representative of uncontrolled flight, and finding appropriate controls is a critical part of designing robotic flyers (22).

To further analyze the stability of flapping flight where the motions of the wings and body are coupled instantaneously, one can apply methods in dynamical systems, in particular, the Floquet stability analysis of periodic systems (10, 22a). A flapping flight due to a periodic wing motion is likely to lead to a periodic orbit in phase space. Each equilibrium flight is a fixed point in the Poincaré map of flight dynamics (**Figure 3**). For longitudinal flight, the phase space is four-dimensional, spanned by U_x, U_z, θ, and ω_b. The periodic flight can be found by searching for an initial state, $\vec{x}_0$, that satisfies the periodic condition $\vec{x}_0 = f(t_0 + qT; t_0, \vec{x}_0)$, where T is the wing-stroke period, q is a fixed integer, and $f(t; t_0, \vec{x}_0)$ evolves the initial state $\vec{x}_0$ to the current state $\vec{x}(t)$. The stability of a periodic flight can be evaluated using a linear stability analysis on the corresponding linear return map. A small perturbation from the equilibrium state, ϵ_0, evolves according to $\epsilon_{n+1} = \nabla f|_{x_0} \cdot \epsilon_n$ to the leading order. The Jacobian matrix of the Poincaré map,
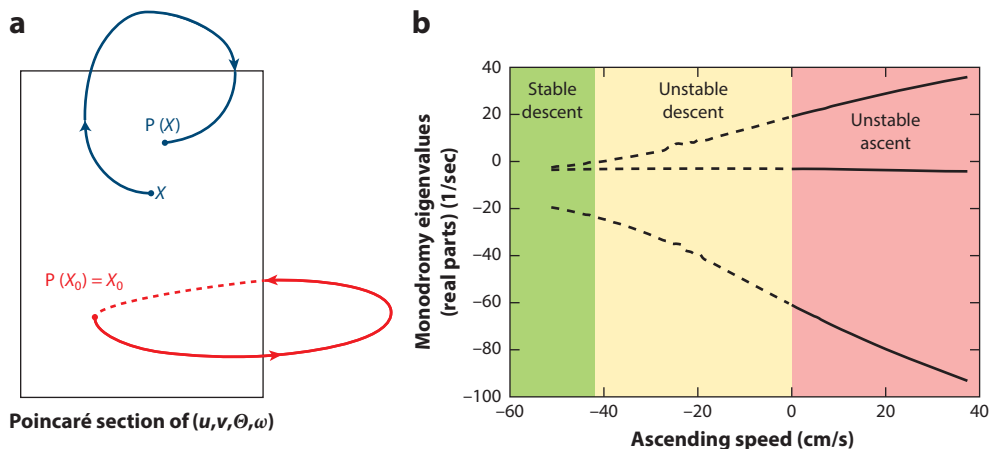
Figure 3

(*a*) The Poincaré map of longitudinal flight. The dynamic state X is four-dimensional, corresponding to two translational velocities and the pitching angle and pitching rate. (*b*) Stability diagram calculated with Floquet stability analyses of periodic flight. For each ascending velocity, the equilibrium state is found by searching for a periodic orbit. The linear stability is given by the eigenvalues of the monodromy matrix. The three curves correspond to the real part of the eigenvalues of the monodromy matrix associated with each periodic flight. Apart from fast descending flight, all have a positive, real eigenvalue corresponding to unsteady flight. Adapted from Reference 22a with permission.

$\nabla f|_{x_0}$, is the monodromy matrix. The periodic flight is stable if and only if all eigenvalues of the monodromy matrix have a modulus less than 1.

In cases where we have examined, for example, when a fruit fly travels at different vertical velocities, corresponding to hovering, ascent, and descent, almost all periodic states are unstable, except at fast descent (**Figure 3**). The pitch instability does not have sensitive dependence on the force coefficients in the aerodynamic force models, but it can be tuned by changing the morphological parameters, such as the position of the wing hinge with respect to the center of the mass of the body.

3. THREE-DIMENSIONAL, FREE-FLIGHT SIMULATIONS WITH FEEDBACK CONTROL

A computational framework for simulating insect flight serves many purposes. In addition to the stability analyses described above, such a framework offers a tool to tease out the causal relations between the observed wing motion and the body dynamics. It also allows us to switch on and off the control algorithms, so as to disentangle the effect from feedback control and the natural flight dynamics. By examining different control schemes, we can gain insight into the algorithms used by insects, as well as obtain theoretical bounds on the timescales for sensing and actuations associated with flight stability and maneuvers.

The building blocks of free-flight simulations include aerodynamic calculations, the dynamic coupling between the body and flapping wings, and the control schemes of wing modulation in response to the measured body dynamics (**Figure 1**).

3.1. Unsteady Aerodynamics

The aerodynamic force on a flapping wing is governed by the Navier-Stokes equations. The fluid velocity $\vec{u}(\vec{x}, t)$ and pressure $p(\vec{x}, t)$ obey the conservation of momentum and mass,

$$\frac{\partial \vec{u}}{\partial t} + (\vec{u} \cdot \nabla)\vec{u} = -\frac{\nabla p}{\rho} + \nu \nabla^2 \vec{u},$$

$$\nabla \cdot \vec{u} = 0,$$

where ρ is the density of the fluid and ν is the kinematic viscosity. By choosing a length scale, L, and velocity scale, U, the equation can be expressed in a nondimensional form containing the Reynolds number, $\mathrm{Re} = \frac{UL}{\nu}$. The flow velocity for these problems is on the order of 1 m/s, which is far smaller than the speed of sound, and thus the flow is nearly incompressible. The coupling between the wing and the fluid lies in the no-slip boundary condition at the wing surface, $\vec{u}_{bd} = \vec{u}_s$, which states that the flow velocity at the wing surface is the same as the wing velocity. Given the wing size and speed, the flow around each flapping wing has a Reynolds number (Re) in the range of 10–10,000. The Re is about 150 for a fruit fly and 3,000 for a dragonfly. The flow is intrinsically unsteady, signified by the formation and shedding of the vortices from the flapping wing (23–25) (**Figure 4**). Understanding the unsteady aerodynamic forces on a flapping wing has motivated many experimental and computational studies (for a review see Reference 28).

For extensive parameter studies, optimization, or back-of-the-envelope calculations, it is also useful to construct reduced-order models of the aerodynamics force. Various models have been proposed in the literature (6, 26, 29–31). The unsteady force on a translating and rotating wing includes three main components. In addition to the quadratic term in the linear velocity, there is also a contribution from the coupling between the rotation and translation, $C_R \vec{U}_w \times \vec{\omega}$, as well as a term due to wing acceleration, $[M_a] \cdot \vec{a}_w$, with $[M_a]$ being the added mass tensor, which depends on the geometry of the wing (32). The added mass term averages to zero for a periodic motion; however, it is relevant when considering instantaneous forces (6). These are quasi-steady forces in the sense that the instantaneous force depends only on the current state of the wing kinematics.

The specific form of the quasi-steady forces that we have used for optimization (33) and for stability analyses (1) are based on our experiments on falling plates in water, which have Reynolds numbers similar to those found in insects (26, 27). Free-falling plates allow us to simultaneously measure the kinematics and unsteady aerodynamic forces, bypassing the use of strain gauges, because the acceleration of the plate is directly proportional to the sum of the aerodynamic force and the gravity. By studying plates with different geometries, one can extract what forces are acting on a plate of arbitrary geometry (26, 34). The force on a 3D wing is typically calculated by evoking the blade-element approximation, which divides the wing into a series of blade elements in the chord direction and then sums up the 2D force on each element. By construction, this ignores the spanwise flow. The difference between these approximated models and the unsteady forces can be studied either by comparing the model force with experiments or with direct numerical simulations (6, 26, 35).

3.2. Newton-Euler Equations for Body and Wing Coupling

The body and wing motions are coupled through the forces and torques at their joints. The aerodynamic force on the wing also depends on the sum of the wing and body velocities. Many methods have been developed for simulating multiple rigid body dynamics. Flapping-flight simulations have either adopted the existing software (36) or solved the explicit dynamic equations for two-winged insects (15). We have chosen a method that treats each of the rigid bodies separately and use kinematic constraints at the joints to determine the internal forces (1). This formulation can be generalized to arbitrary numbers of wings and also lets us include the aerodynamic force terms with ease.
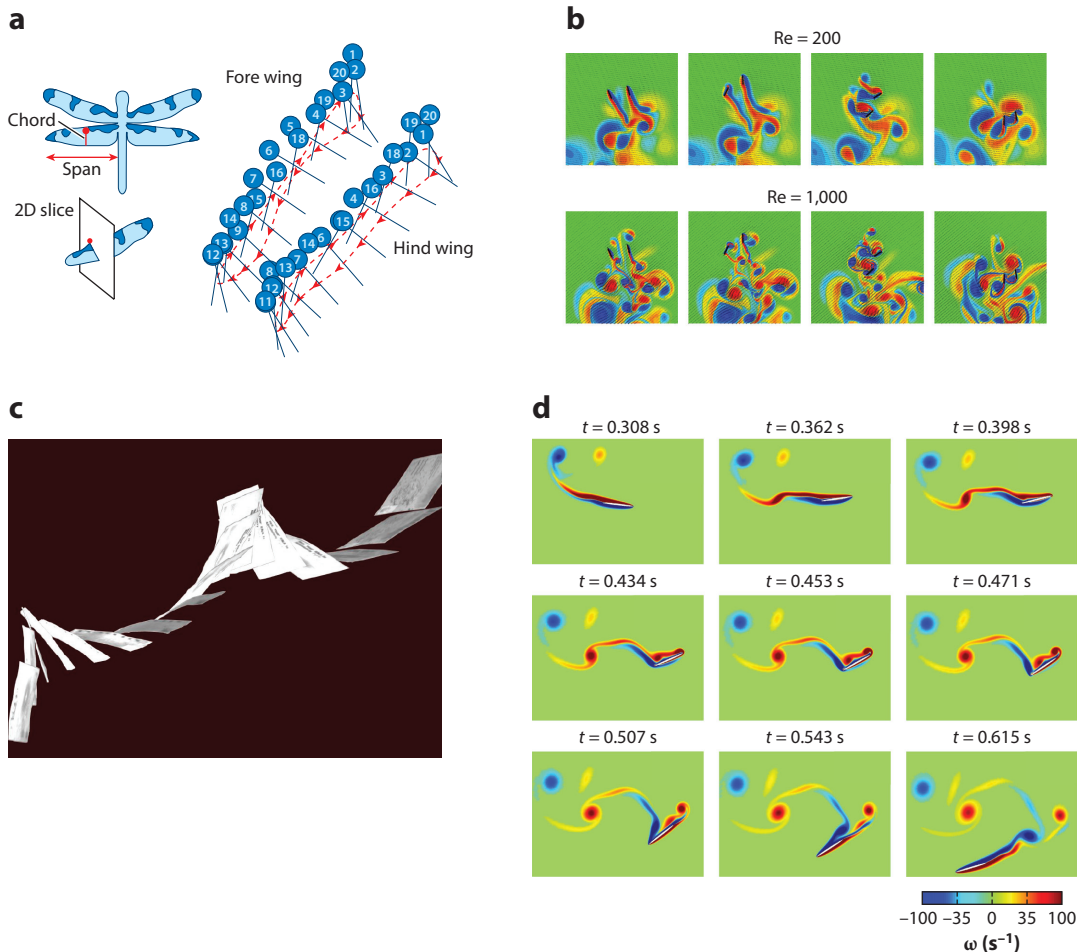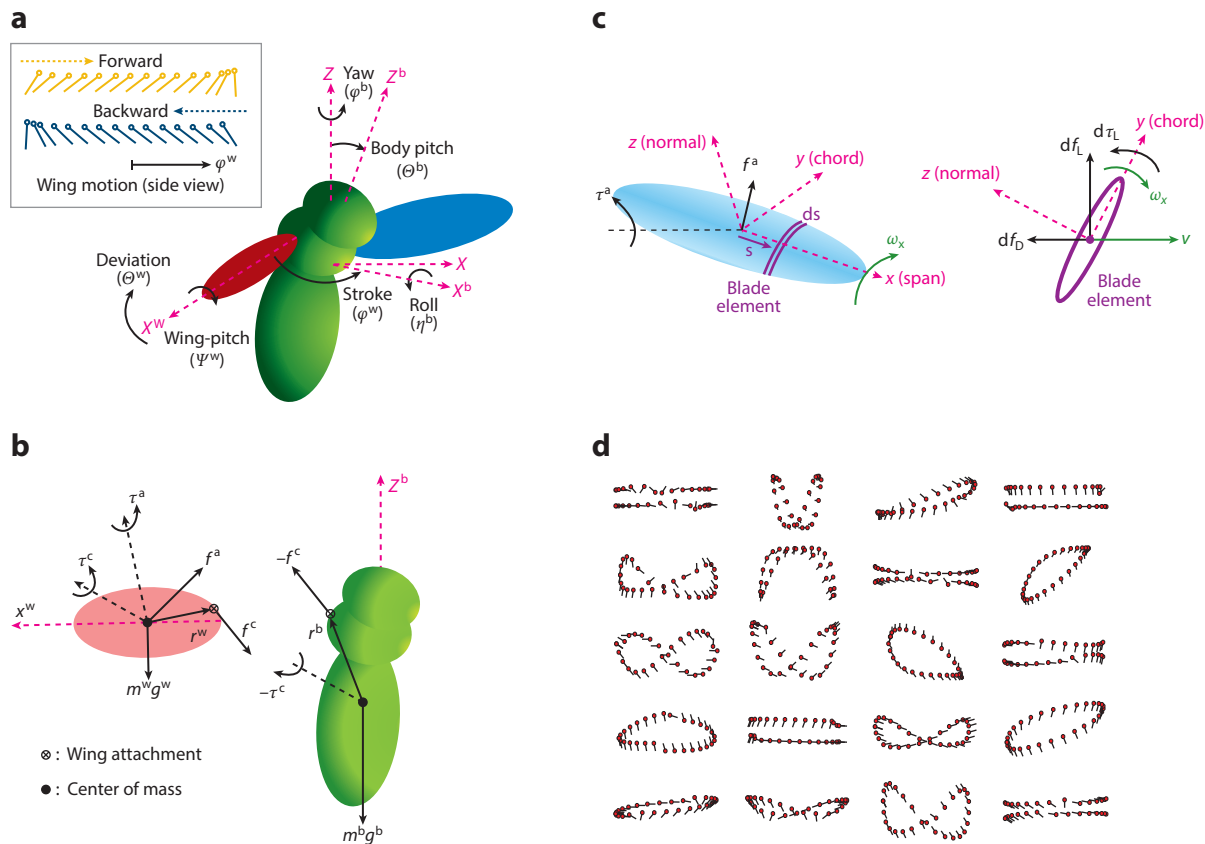
Figure 4

Unsteady aerodynamics. (*a*) Wing kinematics of a dragonfly, with sticks indicting the cross section of a wing viewed from the side.
(*b*) Computed vorticity field around the two wings at two different Reynolds numbers (25). (*c*) Falling paper as an analogous system for
studying the wing and flow interactions. (*d*) Computed vorticity field around a fluttering plate in water at a Reynolds number similar to
those found in insects. The computed forces, together with the experimental measurements, are used to deduce the aerodynamic force
models (26, 27).

The coordinates for each rigid body are defined along its principal axes. The body kinematics
are given by its position $\vec{r}^{\,b}$, linear velocity $\vec{v}^{\,b}$, Euler angles ϕ^b (yaw), θ^b (pitch), η^b (roll), and
the corresponding angular velocity $\vec{\omega}^{\,b}$ (**Figure 5a**). The wing motion is defined relative to the
body and has its own three rotational degrees of freedom, ϕ^w (yaw), θ^w (pitch), and η^w (roll). The
governing equations for the body dynamics are

$$m^b \vec{a}^b = m^b \vec{g} - \sum_{i=1}^{n} \vec{f}^{\,c}_i, \qquad 7.$$

$$\mathbf{I}^b \vec{\beta}^{\,b} = -\vec{\omega}^{\,b} \times (\mathbf{I}^b \vec{\omega}^{\,b}) - \sum_{i=1}^{n} \vec{\tau}^{\,c}_i - \sum_{i=1}^{n} \vec{r}^{\,b}_i \times \vec{f}^{\,c}_i. \qquad 8.$$

Figure 5

Building blocks for 3D free-flight simulation. (*a*) Definition of body and wing rotations. (*b*) Dynamic coupling between the wing and the body. Each is treated separately as a rigid body subject to two constraints at the joint. (*c*) Blade-element approximation for aerodynamic forces on a wing. (*d*) A generic family of wing motions given by Equations 11–13 (33).

Similarly, the governing equations for the ith wing are

$$m_i^{\mathrm{w}} \vec{a}_i^{\mathrm{w}} = m_i^{\mathrm{w}} \vec{g} + \vec{f}_i^{\mathrm{c}} + \vec{f}_i^{\mathrm{a}}, \qquad\qquad 9.$$

$$\mathbf{I}_i^{\mathrm{w}} \vec{\beta}_i^{\mathrm{w}} = -\vec{\omega}_i^{\mathrm{w}} \times \mathbf{I}_i^{\mathrm{w}} \vec{\omega}_i^{\mathrm{w}} + \vec{\tau}_i^{\mathrm{c}} + \vec{r}_i^{\mathrm{w}} \times \vec{f}_i^{\mathrm{c}} + \vec{\tau}_i^{\mathrm{a}}, \qquad\qquad 10.$$

where b and w denote the body and the wing, respectively. m is the mass; $\mathbf{I}$ is the moment of inertia tensor; $\vec{a}$ is the linear acceleration; $\vec{\beta}$ is the angular acceleration; $\vec{g}$ is the gravitational constant; $\vec{\omega}$ is the angular velocity; $\vec{f}^{\mathrm{c}}$ and $\vec{\tau}^{\mathrm{c}}$ are the internal force and torque between the body and the wings, respectively; $\vec{r}_i^{\mathrm{b}}$ is the position of the ith wing-root relative to the body center of mass; and $\vec{r}_i^{\mathrm{w}}$ is the position of the wing relative to the center of mass of the body. Finally, $\vec{f}^{\mathrm{a}}$ and $\vec{\tau}^{\mathrm{a}}$ are the aerodynamic force and torque acting on the wing, respectively.

In these dynamic equations for each rigid body, we have introduced the internal forces and torques at the joints, $\vec{f}^{\mathrm{c}}$ and $\vec{\tau}^{\mathrm{c}}$, which are unknown variables, so we need additional equations that express the kinematic constraints at the joints. There are two constraints at each joint connecting a wing to the body. The first is on the angular acceleration of the wing relative to the body, $\vec{\beta}_i^{\mathrm{r}} = \vec{\beta}_i^{\mathrm{w}} - \vec{\beta}^{\mathrm{b}}$, which must agree with the prescribed wing motion. The second is the

matching condition for the linear acceleration of the wing and the body at the attachment point: $\vec{a}^{\,b} + \vec{\beta}^{\,b} \times \vec{r}_i^{\,b} + \vec{\omega}^{\,b} \times (\vec{\omega}^{\,b} \times \vec{r}_i^{\,b}) = \vec{a}_i^{\,w} + \vec{\beta}_i^{\,w} \times \vec{r}_i^{\,w} + \vec{\omega}_i^{\,w} \times (\vec{\omega}_i^{\,w} \times \vec{r}_i^{\,w})$. The main difference between this set of equations and the averaged dynamic models described earlier lies in the treatment of the instantaneous inertial coupling between the wing and the body. In the averaged model, the wing inertia is ignored, and the aerodynamic force is averaged over a cycle. Here, the Newton-Euler equations, together with the aerodynamic force modeling, provide a general method for simulating flapping flight in 6 degrees of freedom. The special cases of yaw, pitch, and roll dynamics are subsets in this framework. For the stability analysis of periodic orbits, these equations serve as the evolution operator, $f(t; t_0, \vec{x}_0)$, in the Floquet analysis.

3.3. Wing Motions

Flies, bees, and hummingbirds use similar reciprocal wing strokes. They flap their wings back and forth about an approximately horizontal stroke plane (**Figure 1b**). The wing tips trace out a figure eight or an elliptical-shaped orbit, and the wing can twist about its spanwise axis (37, 38). The wing motion is similar to the strokes we use to tread water, but with the leading edge leading in both the forward and backward strokes. The frequency for different insect range from a few hertz to about 800 Hz. The smaller the insect, the faster it beats its wings. The frequency roughly scales with the inverse of the wing length (24, 39). A fruit fly beats its wings at about 250 Hz, a dragonfly at about 40 Hz, and a butterfly at about 15 Hz.

The need for accurate and efficient methods for tracking animal motion has driven recent development of various algorithms for 3D tracking of insect wing and body dynamics (40–43). They offer increasingly refined kinematic descriptions and have become indispensable tools for animal research. For modeling, it is also useful to abstract the wing motions into a family of periodic functions. We can construct three periodic functions, one for each rotational degree of freedom: $\phi^w(t)$, the stroke angle; $\theta^w(t)$, the deviation angle; and $\psi^w(t)$, the wing-pitch angle (33):

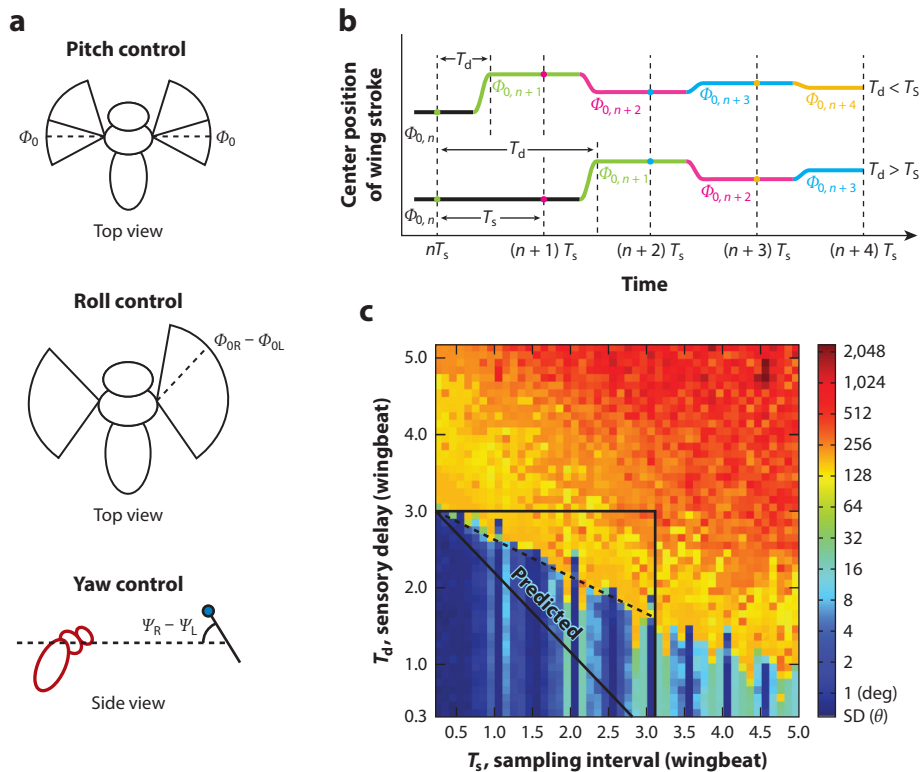$$\phi^w(t) = \phi_0 + \phi_m \frac{\arcsin[K\sin(2\pi f t)]}{\arcsin K}, \tag{11.}$$

$$\theta^w(t) = \theta_0 + \theta_m \cos(N \cdot 2\pi f t + \delta_\theta), \tag{12.}$$

$$\psi^w(t) = \psi_0 + \psi_m \frac{\tanh[C\sin(2\pi f t + \delta_\psi)]}{\tanh C}, \tag{13.}$$

where ϕ_0, θ_0, and ψ_0 are the constant offsets and ϕ_m, θ_m, and ψ_m are the amplitudes. f is the wingbeat frequency, δ_θ and δ_ψ are the phase shifts, and $N = 1$ or 2, $0 < K < 1$, $C > 0$ are waveform control parameters. $N = 1$ corresponds to one vertical oscillation per stroke, and $N = 2$ corresponds to a figure eight motion. ϕ becomes sinusoidal when K is close to 0 and triangular when K is close to 1. ψ approaches sinusoidal form for small C and a step function for large C. Examples of the wing strokes in this family are shown in **Figure 5d**.

3.4. Feedback Control Algorithms

The neural control of the body posture during flight is modeled by feedback control algorithms that specify the wing kinematic changes in response to the measured dynamic state of the body. There are potentially different approaches to constructing these control algorithms. One could start from the control literature and view insect flight as a special example of general control problems. The approach we followed is to extract some key elements from the behavioral studies

a

Pitch control

Φ_0 Φ_0

Top view

Roll control

$\Phi_{0R} - \Phi_{0L}$

Top view

Yaw control

$\Psi_R - \Psi_L$

Side view

b

Center position of wing stroke

T_d

$\Phi_{0, n+1}$ $\Phi_{0, n+2}$ $\Phi_{0, n+3}$ $\Phi_{0, n+4}$ $T_d < T_S$

$\Phi_{0, n}$

T_d

$\Phi_{0, n+}$ $\Phi_{0, n+1}$ $\Phi_{0, n+2}$ $\Phi_{0, n+3}$ $T_d > T_S$

$\Phi_{0, n}$ T_s

nT_s $(n+1)T_s$ $(n+2)T_s$ $(n+3)T_s$ $(n+4)T_s$

Time

c

T_d, sensory delay (wingbeat)

Predicted

T_s, sampling interval (wingbeat)

2,048
1,024
512
256
128
64
32
16
8
4
2
1 (deg)
SD (θ)

Figure 6

Control algorithm and timescales. (*a*) Both pitch and roll can be controlled by shifting the stroke forward and backward. The body pitch can be controlled by shifting the center of the wing stroke symmetrically between left and right wings, and the body roll can be controlled by shifting the strokes asymmetrically. Body yaw can be controlled by changing the relative wing pitch between left and right wings (2, 19). (*b*) Discrete time-delayed controller for the body pitch. It takes measurements every T_s, and reacts after T_d. Time is measured in wingbeats. (*c*) Controllability as a function of sensing rate, every T_s wingbeats, and time delay between sensing and action, T_d. The color corresponds to the root-mean-square value of body pitch. Blue indicates well-controlled flight.

of the fly's response to perturbations. The control analyses can then lead to interpretations of experimental results and offer predictions to be tested by further experiments.

To remain stable and to maneuver, insects have developed different strategies to modulate their wing motion so as to generate the necessary forces and torques to accelerate and to turn. As we saw earlier, the aerodynamic force depends on a number of parameters in the wing motion: the amplitude, the frequency, the angle of attack, and the detailed time course in the three degrees of freedom of wing rotation. Although a typical set of wing kinematics contains a complex mix of changes in all these variables, it is possible to discern some of the correlations between the observed wing and body kinematics that are consistent with our intuition about the direction of the aerodynamic forces and torques (**Figure 6*a***).

For example, to pitch the body, a fly can shift the center of its wing strokes forward and backward to adjust the averaged positions of the aerodynamic forces relative to the center of its mass (44). To roll about the body's long axis, a fly can use asymmetric amplitudes to generate a

differential lift, and to yaw, it can use asymmetric angles of attack to generate differential drag for the yaw torque (2, 8, 19, 42, 45).

Using pitch control as an example, we can construct a discrete time-delayed control algorithm that senses the body state at discrete intervals of T_s and adjusts the center of the wing stroke, ϕ_0, according to the body-pitch (θ_b) and body-pitching rate, ω_b, measured at a previous time, $\phi_0(t) = k_\theta \theta_b(t - T_d) + k_\omega \omega_b(t - T_d)$ (**Figure 6b**). This controller can be viewed as a proportional-integral control, with ω_b directly sensed by the halteres (Section 5.1) and θ_b being ω_b's integration over time. Using such an algorithm, we can make a model insect hover stably (see **Video 2**) (1).

Similar algorithms can be constructed for other degrees of freedom (**Figure 6a**). Instead of ϕ_0, we can use the amplitude difference between left and right wings for roll and wing pitch asymmetry for yaw. For vertical translation, we can make symmetric changes in the wing-stroke amplitude. The transverse motion is coupled with the rotation of the body, as we saw in the stability analysis. The sideways motion occurs together with the rolling motion, and the forward translation accompanies the pitching motion. In a typical flight, because different degrees of freedom are coupled, a combination of these wing adjustments is necessary for a desired maneuver. The main features of the control algorithms considered here are that they are discrete in time, both in sensing and in action, and they are linear functions of the dynamic state of the body at a prior time.

4. A PREDICTION OF THE SENSING RATE FOR STABLE FLIGHT

With closed-loop simulations, we can determine how fast and how often the feedback control should sense and act in order to stabilize flapping flight. The discrete time-delayed control introduces two new timescales to the problem, the sensing rate, T_s, and the delay time, T_d. Their effects on the control of the flight are summarized in the phase diagram (**Figure 6c**), which reveals two key results. First, for each sensing rate, there is a critical time delay below which the flight can be controlled. Second, the most effective control occurs at sampling intervals that are integer multiples of half a wingbeat, $T_s = 0.5, 1, \ldots$ wingbeats.
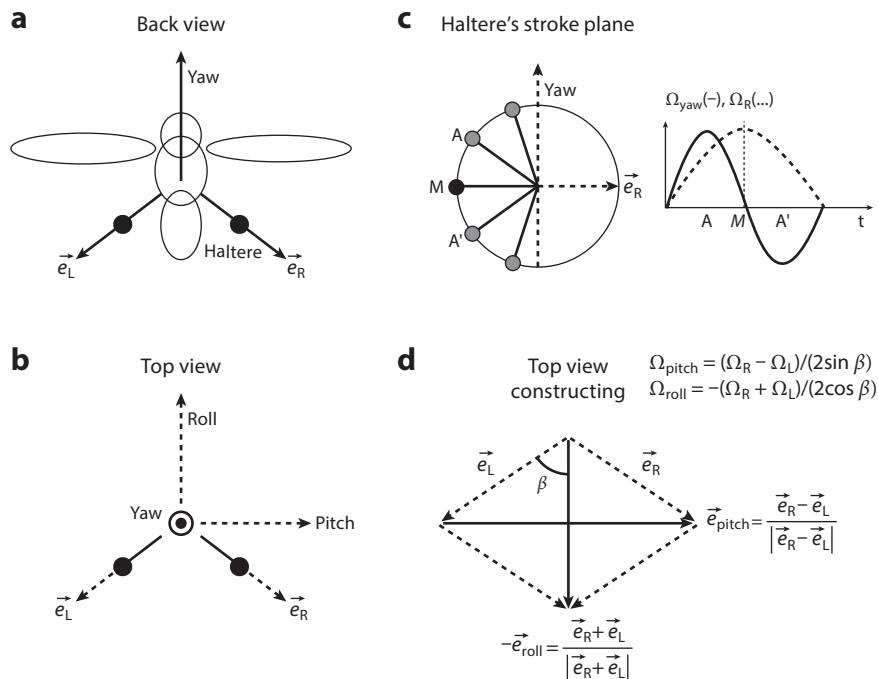
This sensitivity to discrete values of T_s reflects the beat-to-beat oscillation of the underlying time-periodic system. It is more effective for the flies to clock their sensing and actuations by wingbeats, for example, to initiate turns by adjusting the wing motion at the two ends of a stroke, and to switch on and off the actuations in discrete time steps. The discrete control was seen also in the analyses of a fruit fly's yaw turn. The fly switches gears, modeled as a torsional spring, in a step-function-like fashion (2). These finer-scale control strategies deserve further investigation.

The phase diagram also shows that the control is most robust in the vicinity of $T_s = 1$, and this led us to conjecture that a fly senses its body rotation every wingbeat for stability (1). Relating the timescales required for flight stability to the findings in neurophysiology of the fly's reflex for balance further led us to conjecture that one of the fly's seventeen steering muscles, the first basalar muscle (Mb1), is the key muscle for regulating flight stability. To see these connections, we next discuss the literature on halteres and the associated neural-feedback circuitry.

5. A FLY'S STABILITY REFLEX: HALTERES, MOTOR NEURONS, AND STEERING MUSCLES

5.1. Halteres as Gyroscopic Sensors for Body Rotation

For a fruit fly, a beat-to-beat sensing rate means a measurement every 4 ms. Even in the world of small, this is fast. For comparison, the timescales for visual feedback circuitries in insects are in the

a Back view

c Haltere's stroke plane

b Top view

d Top view constructing

$\Omega_{\text{pitch}} = (\Omega_R - \Omega_L)/(2\sin\beta)$
$\Omega_{\text{roll}} = -(\Omega_R + \Omega_L)/(2\cos\beta)$

$$\vec{e}_{\text{pitch}} = \frac{\vec{e}_R - \vec{e}_L}{|\vec{e}_R - \vec{e}_L|}$$

$$-\vec{e}_{\text{roll}} = \frac{\vec{e}_R + \vec{e}_L}{|\vec{e}_R + \vec{e}_L|}$$

Figure 7

Halteres' detection of body rotation. (*a,b*) A pair of halteres tucked behind the main wings. They point backward by about 30° and beat along a vertical stroke plane. (*c*) The Coriolis force normal to the stroke plane encodes Ω_y and $\Omega_{L,R}$. The signal corresponding to Ω_y oscillates at twice the frequency of the wingbeats, peaking at the quarter stroke (A,A'), and the signal corresponding to $\Omega_{L,R}$ oscillates at the frequency of the wingbeats, peaking at the midstroke (M). (*d*) The vector sum and difference of the two lateral axes, one for each haltere, $\vec{e}_L$ and $\vec{e}_R$, leading to two orthogonal axes, corresponding to the body roll and pitch directions, $-\vec{e}_{\text{roll}}$ and $\vec{e}_{\text{pitch}}$, respectively. It follows that $\Omega_{\text{pitch}} = (\Omega_R - \Omega_L)/(2\sin\beta)$ and $\Omega_{\text{roll}} = -(\Omega_R + \Omega_L)/(2\cos\beta)$.

range of 20–50 ms (46, 47). A fast sensor on a fly is a pair of halteres, which are mechanosensors evolved from the fly's hindwings. They detect the rotation of the body by sensing the small Coriolis force exerted on them and provide direct neural signals to the motor neurons of steering muscles (47–49). Each haltere is a thin stalk with a thick end-knob (**Figure 7**). They oscillate at the same frequency as the forewings but in antiphase. The role of halteres in flight stability was first reported by Derham in 1713, who saw that the flies would tumble and fall without their halteres (50). Attaching a thread to a fly's abdomen would, however, restore its stability. This and other behavioral evidence led Fraenkel & Pringle to suggest that the halteres act as a pair of gyroscopes for flight stabilization (51). The gyroscopic mechanisms were initially worked out in an analysis by Pringle in 1948 (52) and were further elaborated in a series of behavioral studies of the head-response of tethered flies subject to accelerations (53–55).

The sensing mechanism is based on the detection of the Coriolis force acting on a flapping stalk with an end-knob mounted on a rotating body, much like a Foucault pendulum. The Coriolis force, $2\vec{U}_w \times \vec{\Omega}_b$, is proportional to the haltere velocity, $\vec{U}_w$, and to the body rotation, $\vec{\Omega}_b$. The small Coriolis force on the end-knob is measured at the haltere's base by a group of directional mechanoreceptors, campaniform and codototal sensilla (49). The orientation of the sensilla as well

as the fly's response to imposed accelerations suggest that they primarily detect the force normal to the stroke plane (52, 55, 56).

Two questions related to flight control are how a fly makes use of the Coriolis force to deduce the rotational rate of its body and how it responds by modulating its wing strokes. One can ask whether flies construct independent control algorithms in response to the rotational rate along the symmetrical axes of the body: the roll, yaw, and pitch directions (47, 55). Behavioral studies, including the earlier observation of free flight (49, 57) and later more systematic studies of tethered flight (54, 55), have shown that flies respond to rotations in all three directions with different wing kinematic changes. By measuring the Coriolis force normal to the stroke plane, each haltere can detect the two components of the angular velocity in the stroke plane. Because the two stroke planes are not coplanar, in theory, all three components of the angular velocity can be detected.

The decomposition can be done in multiple ways. Here I give an algorithm in response to questions concerning the role of the in-plane noninertial forces and the effect of the two nonorthogonal stroke planes (55). The decomposition involves two steps (**Figure 7**). As noted in Reference 52, the normal force on each haltere encodes Ω_y, angular velocity along the yaw axis, and $\Omega_{L,R}$ along the lateral axes. Ω_y and $\Omega_{L,R}$ can be separated according to their different frequencies: The signal due to Ω_y oscillates at twice the wing frequency, whereas the signal due to $\Omega_{L,R}$ oscillates at the wing frequency. The separation can be done without using a Fourier transform, for example, by taking phase-locked measurements, or by averaging over different portions of the strokes. The sum of the two consecutive quarter strokes only depends on $\Omega_{L,R}$, and the difference only depends on Ω_y (**Figure 7c**). If different groups of campaniform sensilla are already tuned to detect different frequencies, then we can bypass this initial step. With the two signals from each haltere, the fly can combine them to extract all three components of rotation. For yaw, we take the average of the two and this will reduce the noise. For pitch, Ω_p, and roll, Ω_r, we can take the sum and difference of Ω_R and Ω_L, weighted by geometric factors $1/(2\sin\beta)$ and $-1/(2\cos\beta)$, respectively (**Figure 7d**). This follows from the fact that the vector sum and difference of any pair of unit vectors lead to a pair of orthogonal axes, and the sum of the unit vectors along the two lateral axes give a pair of orthogonal axes in the pitch and yaw directions. Note that these vector operations do not require the two stroke planes to be orthogonal. A rotation of the coordinates, however, would require the orthogonality of the stroke planes (54). Also, because only the Coriolis force normal to the stroke plane is needed, it avoids the interference from other larger in-plane forces, the centrifugal force and the force due to linear acceleration.

To find out whether flies use algorithms similar to this would require further experiments. So far, the physiological studies have yet to offer direct support for a bilateral computation (56, 58). However, the anatomy of haltere afferents in the blowfly show prominent lateral branches in the metathorax (59, 60), making them likely candidates for cross-computations.

Short of bilateral computations, there is another possibility for flies to control their three axes of rotation, without computing the pitch and roll separately. Suppose that each haltere only sends its signal to the steering muscles for one wing, resulting in a small change in the wing kinematics. In the dynamic regimes where the body responds linearly to a small adjustment of the wing motion, the summation of the signals from the two halteres can effectively take place in the body dynamics rather than in the neural circuitry. Given that most turning maneuvers, including more dramatic saccades, result from relatively small changes in the wing strokes (2, 19, 48), the linear response is likely to hold for many maneuvers. As seen in recent studies of flies' yaw turns in response to torque perturbations, the corrective body rotational angle has a linear dependence on the wing pitch asymmetry (19). Moreover, the effective torque needed to generate a large yaw turn is proportional to the wing pitch asymmetry (2). These linear relations between the wing and

body kinematic changes reflect an efficient scheme to control the body dynamics, a point that I shall return to.

5.2. Sensing Rate, Motor Neurons, and Steering Muscles

The next question is how the signals from the halteres affect the wing kinematics. Starting with the sensors at the haltere base, the strain caused by the Coriolis force alters the firing patterns of the campaniform sensory neurons (52, 61). These sensory neurons are connected to the motor neurons. Although not all of the connections have been mapped out, the first basalar muscle (Mb1), one of the steering muscles, has a beat-to-beat firing pattern (62–64). Moreover, it is active even during steady flight, whereas other muscles are active during turning maneuvers in response to visual stimuli (63, 64). The beat-to-beat firing pattern suggests an input from afferents from haltere and wing nerves (64). Intraceullar neural recordings have further found that the connection between haltere nerves and the motor neuron is monosynaptic, suggesting a fast neural pathway between the haltere sensors and the motor neuron for the first basalar muscle (62, 65).

In addition to the signals from the halteres, the motor neurons to the steering muscles also receive strong visual inputs. In fact, a moving visual display is the dominant method for eliciting turning response in flies (21, 58, 66, 67). By eliciting a fly's attempts to turn while being tethered, it is possible to make neural recordings. This further allows for a close examination of the correlations between the muscle activity of specific muscles and wing kinematic changes (63). Electrophysiological experiments in *Drosophila* have shown that three of the largest steering muscles (Mb1, Mb2, and MI1) can account for many of the changes in wing motion during saccades and other maneuvers (63, 68). The large changes in stroke amplitude from one stroke to the next are associated with the activity of Mb2 and MI1, whereas the more subtle changes in the wing strokes are correlated with the firing phase of Mb1.

5.3. A Conjecture on the Role of the First Basalar Muscle in Flight Stability

Viewing these results together with the phase diagram for flight stability, we suggested that the main function of the first basalar muscle is to counter instability during steady flight (**Figure 8**) (1). It responds to signals from the halteres at every wingbeat by making a small adjustment in the wing motion to shift the center position of the stroke. Moreover we expect that wing kinematic changes are made to correct the two unstable directions of flight, pitch, and roll. In theory, the corrections in pitch and roll can be done with the same variable, the shift in the wing-stroke position forward and backward with respect to the insect's center of mass. A symmetric shift between the left and right wings would correct for a pitch instability, and an asymmetric shift that leads to asymmetric amplitude between the left and right wings can correct for a roll instability (**Figure 6a**).

5.4. Initial Observations of Flies with the MNb1 Motor Neuron Silenced

Only small kinematic changes in the wing are needed to correct for instability. A change of a fraction of a degree in the wing stroke is sufficient (1). This makes it difficult to discern the effect of Mb1 on wing kinematics during steady flight based on direct observation. So far, the kinematic changes in the wing have been studied in turning maneuvers, where the asymmetry is on the order a few degrees, which is small but measurable. One recent development in neural science is the ability to alter specific neural circuitries with genetic modifications. Flies with their motor neurons to the first basalar muscle (MNb1) silenced just became available. This allows us to examine flight behavior when the Mb1 muscle does not receive direct inputs from the haltere. An initial comparison between these genetically modified flies and the control group is shown in

Back view

Haltere (gyroscopic sensor)

Haltere

Motor neuron (MNb1) of first basalar muscle

Mb1
Mb2

MNb1 adjusts the tension of Mb1

Modifies the wing motion

**Corrects for body rotation
to stabilize flight**
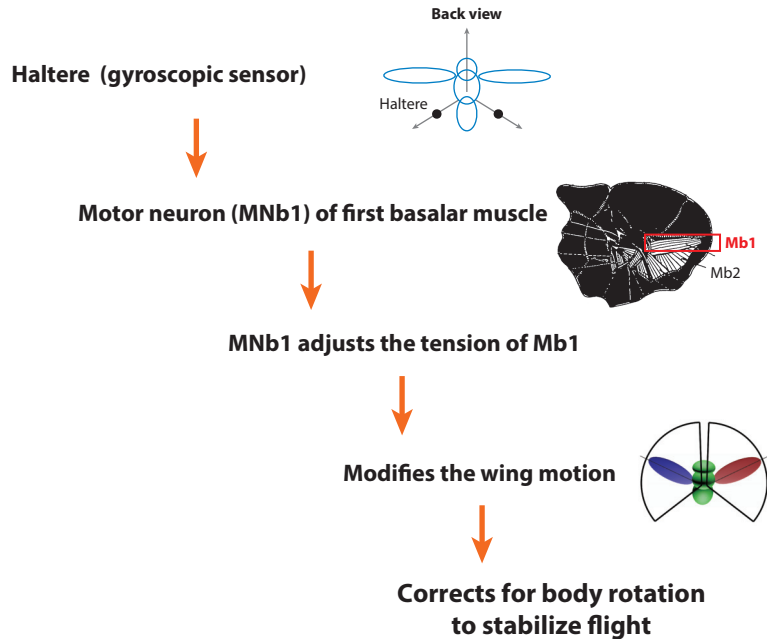
Figure 8

A fly's stability reflex during steady flight: from halteres to wing adjustment. Flies have two distinct groups of flight muscles: large asynchronous muscles attached to the thorax to drive the wings at high frequency via resonance and 17 pairs of small steering muscles directly attached to each wing to adjust the wing motion (73, 74, 77). The first basalar muscle is one of the steering muscles.

Figure 9. The flies with the MNb1 motor neuron silenced fall at a much faster rate and have trouble stabilizing their body pitch. A more careful statistical quantification is under way (69). This work is a new step toward understanding the functional role of a fly's steering muscles during free flight.

6. FURTHER THOUGHTS

6.1. A Fly's Gearbox

The first basalar muscle is one of the seventeen small steering muscles directly attached at the base of each wing. The function of a fly's muscles has long been a subject of interest in anatomical studies (49, 70–73) and neurophysiological studies (64, 68, 74), as well as X-ray imaging (75, 76). In Diptera, the steering muscles are separated from the power muscles (49, 77, 78). The wings are driven by a set of large powerful asynchronous muscles attached to the thorax. Although these power muscles are now textbook examples of an insect's solution for generating high-frequency flapping motions by making use of the stiff thorax as a resonating box, the specific functions of the small steering wing muscles during flight maneuvering require further study. The neuroanatomical studies of fly's muscles have provided an initial map on a subset of muscles based on the correlation between the pull of the muscles and the change in the wing kinematics (74, 77). Silencing specific motor neurons of each of these steering muscles provides a new possibility for observing the consequence of the missing action of an individual muscle on flight dynamics during free flight. The 3D wing and body tracking of these flight behaviors would provide data on the correlation
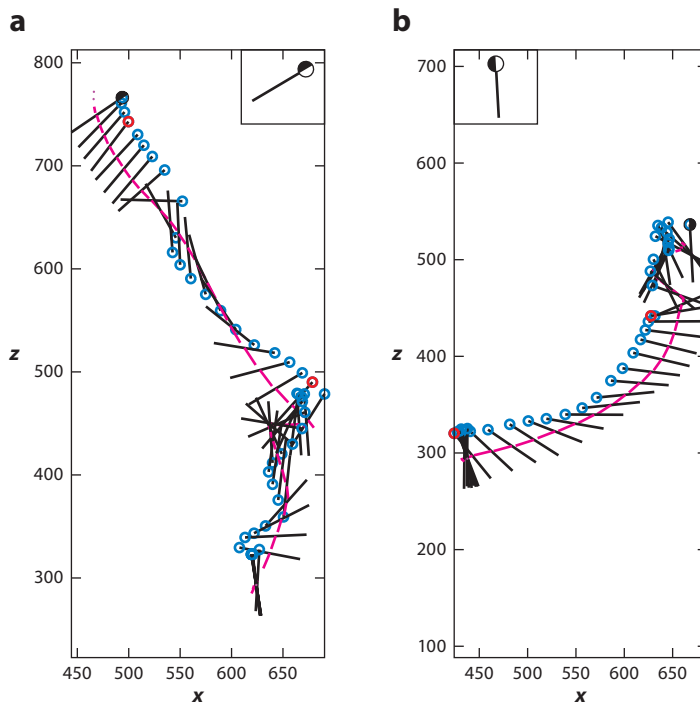
Figure 9

Comparison of flight trajectories of (*a*) a fly with its MNb1 motor neuron silenced and (*b*) a normal fly in the control group. The flies with silent MNb1 tend to have erratic trajectories and steeper falls (69).

between the muscles and kinematics of the wings. Dynamic calculations of free flight will provide a means to tease out the causal relations between observed body dynamics and wing kinematic changes, and therefore are critical to our understanding of the gear mechanisms.

One would hope that in spite of the complex relationships among the muscles that tug and pull the wings, the key mechanisms for flight control can be understood with relatively few variables. It is this belief that drives our modeling efforts. Our previous analysis of saccades found that the turning dynamics of the body can be explained in terms of a small shift in the equilibrium position of a torsional spring at the wing hinge (2, 79). Here the analyses of flight stability single out one of the steering muscles on stability in steady flight.

6.2. From Small to Large, Hierarchical Organization, Dynamical Equilibria, and Links Among Different Parts

By definition, a complex system has many parts. "Why are atoms so small and we so large?" as Schrödinger asked in his set of lectures on "What Is Life?" (80). Take neurons alone: Each of us has about 100 billion neurons, a fly has 700,000, and a small worm, *Caenorhabditis elegans*, has 302 (81). Why do we need so many? How are these neurons organized to carry out specific computations?

The flight stability reflex discussed here is a circuitry small enough for us to comprehend, and it offers some insights into the organization of the neural computation for motion. We can imagine a hierarchical organization within the organism composed of mechanical, chemical, and computational units. Each subsystem has evolved to be near a dynamic equilibrium. Animals' actions are likely the result of small perturbations away from that equilibrium, passing from one

level to another. We can further imagine that the equilibrium is marginally unstable. Small changes lead to small changes if the system is slightly unstable. So it is conceivable that flight maneuvers, spectacular as they are, arise from a succession of linear transformations.

To reiterate the sequence of a fly's balancing act in these terms, the body's initial rotational rate causes a proportional small strain, which leads to a proportional change in muscle stiffness, and a subsequent proportional shift in the wing strokes, which further leads to a proportional change in the rate of rotation of the body. All together, the final change in the body rotation is linearly proportional to the initial change, or $d\vec{\Omega}(t + \tau_d) = M_1 M_2 .... M_n \, d\vec{\Omega}(t)$, with M_i representing linear transformations.

6.3. Theory and Experiments

Finally, few parts of a living system are amenable to descriptions and analyses based on first principles, and not surprisingly, studies of animal behavior have largely been experimental. In the case of insect flight, by including the laws of movement, we start to build a theoretical framework to interpret and predict the functions and designs of insects' internal machinery. These predictions can be tested experimentally by modifying specific neurons in animals, thanks to advances in genetics. This is an encouraging and exciting development.

DISCLOSURE STATEMENT

ACKNOWLEDGMENTS

LITERATURE CITED

1. Chang S, Wang ZJ. 2014. *PNAS* 111(31):11246–51
2. Bergou AJ, Ristroph L, Guckenheimer JM, Cohen I, Wang ZJ. 2010. *Phys. Rev. Lett.* 104:148101
3. Collins S, Ruina A, Russ T, Martijn W. 2005. *Science* 307:1082–85
4. Cook MV. 1997. *Flight Dynamics: Principles*. London: Arnold
5. Etkin B. 1983. *Dynamics of Flight Stability and Control*. Hoboken, NJ: John Wiley and Sons
6. Wang ZJ, Birch JM, Dickinson MH. 2004. *J. Exp. Biol.* 207:449–60
7. Prandtl L, Tietjens OG. 1934. *Applied Hydro- and Aeromechanics*. New York: McGraw-Hill
8. Beatus T, Guckenheimer JM, Cohen I. 2015. *J. R. Soc. Interface* 12(105):20150075
9. Ristroph L, Ristroph G, Morozova S, Bergou AJ, Chang S, et al. 2013. *J. R. Soc. Interface* 10(85):20130237
10. Wu JH, Sun M. 2012. *J. R. Soc. Interface* 9(74):2033–46
11. Faruque I, Humbert JS. 2010. *J. Theor. Biol.* 264:538–52
12. Sun M, Wang JK. 2007. *J. Exp. Biol.* 210:2714–22
13. Sun M, Xiong Y. 2005. *J. Exp. Biol.* 208:447–59
14. Taylor GK, Thomas ALR. 2003. *J. Exp. Biol.* 206:2803–29
15. Sun M. 2014. *Rev. Mod. Phys.* 86:615

16. Cheng B, Deng X. 2011. *IEEE. Trans. Robot.* 27:849
17. Hedrick TL, Cheng B, Deng X. 2009. *Science* 5924:252–55
18. Hesselberg T, Lehmann FO. 2007. *J. Exp. Biol.* 210:4319–34
19. Ristroph L, Bergou AJ, Ristroph G, Coumes K, Berman G, et al. 2010. *PNAS* 107(11):4820–24
20. Fry SN, Sayaman R, Dickinson MH. 2003. *Science* 300:495–98
21. Reichardt W, Poggio T. 1976. *Q. Rev. Biophys.* 9:311–75
22. Ma KY, Chirarattananon P, Fuller SB, Wood RJ. 2013. *Science* 340(6132):603–7
22a. Chang S, Wang ZJ. 2011. *The timing in the control of insect flight instability*. Presented at Annu. Meet. APS Fluid Dyn., 64th, Baltimore
23. Wang ZJ. 2000. *J. Fluid Mech.* 410:323–41
24. Wang ZJ. 2000. *Phys. Rev. Lett.* 85(10):2035
25. Wang ZJ, Russell D. 2007. *Phys. Rev. Lett.* 99:148101
26. Andersen A, Pesavento U, Wang ZJ. 2005. *J. Fluid Mech.* 541:65–69
27. Pesavento U, Wang ZJ. 2004. *Phys. Rev. Lett.* 93(14):144501
28. Wang ZJ. 2005. *Annu. Rev. Fluid Mech.* 37:183–210
29. Ellington CP. 1984. *Philos. Trans. R. Soc. Lond. B* 305:1–181
30. Sane S. 2003. *J. Exp. Biol.* 206:4191–208
31. Weis-Fogh T, Jensen M. 1953. *Proc. R. Soc. B* 239:415–58
32. Lamb H. *Hydrodynamics*. Cambridge, UK: Cambridge Univ. Press
33. Berman G, Wang ZJ. 2007. *J. Fluid Mech.* 582:153–67
34. Varshney K, Chang S, Wang ZJ. 2012. *Nonlinearity* 25:C1–8
35. Wang ZJ. 2004. *J. Exp. Biol.* 207:4147–55
36. Dickson WB, Straw AD, Dickinson MH. 2008. *AIAA J.* 46(9):2150–64
37. Dalton S. 1975. *Borne on the Wind*. New York: Reader's Digest
38. Marey EJ. 1868. *C. R. Acad. Sci. Paris* 67:1341–45
39. Greenewalt CH. 1962. *Dimensional relationships for flying animals*, Vol. 144, No. 2, Smithson. Misc. Coll., Washington, DC
40. Fontaine EI, Zabala F, Dickinson MH, Burdick JW. 2009. *J. Exp. Biol.* 212:1307–23
41. Hedrick TL. 2008. *Bioinspir. Biomimet.* 3:034001
42. Ristroph L, Berman GJ, Bergou AJ, Wang ZJ, Cohen I. 2009. *J. Exp. Biol.* 212:1324–35
43. Walker SM, Thomas ALR, Taylor GK. 2009. *J. R. Soc. Interface* 6:351–66
44. Hollick FSJ. 1940. *Philos. Trans. R. Soc. B* 230:357–90
45. Cheng B, Deng X, Hedrick TL. 2011. *J. Exp. Biol.* 214:4092–106
46. Land M, Nilsson DE. 2012. *Animal Eyes*. Oxford, UK: Oxford Univ. Press
47. Taylor GK, Krapp HG. 2007. *Adv. Insect Physiol.* 34:231–316
48. Dickinson MH. 2005. *Integr. Comp. Biol.* 45:274–81
49. Pringle J. 1957. *Insect Flight*. Cambridge, UK: Cambridge Univ. Press
50. Derham W. 1713. *Physico-Theology (Boyle lecture for 1711)*. London: W. Innys
51. Fraenkel G, Pringle JWS. 1938. *Nature* 141:919–20
52. Pringle JWS. 1948. *Philos. Trans. R. Soc. B* 233(602):347–84
53. Nalbach G. 1993. *J. Comp. Physiol. A* 173:299–304
54. Nalbach G. 1994. *Neuroscience* 61:155–63
55. Nalbach G, Hengstenberg G. 1994. *J. Comp. Physiol. A* 175:708–9
56. Sandeman DC, Markl H. 1980. *J. Exp. Biol.* 202:1481–90
57. Faust R. 1952. *Zool. Jahr.* 63:325–66
58. Dickinson MH. 1999. *Philos. Trans. R. Soc. Lond. B* 354:973–80
59. Chan WP, Dickinson MH. 1996. *J. Comp. Neurol.* 369:405–18
60. Strausfeld NJ, Seyan HS. 1985. *Cell Tissue Res.* 240:601–15
61. Pflugstaedt H. 1912. *Z. wiss. Zool.* 100:1–59
62. Fayyazuddin A, Dickinson MH. 1996. *J. Neurosci.* 16:5225–32
63. Tu MS, Dickinson MH. 1996. *J. Comp. Physiol.* 178:833–45
64. Heide G. 1983. *BIONA report*, Vol. 2, ed. W Nachtigall, pp. 35–52. Mainz, Ger.: Gustav Fischer Akad. Wiss.

65. Fayyazuddin A, Dickinson MH. 1999. *J. Neurophysiol.* 82:1916–26
66. Mayer MK, Vogtmann B, Bausenwein R, Wolf R, Heisenberg M. 1988. *J. Comp. Physiol. A* 163:389–99
67. Sherman A, Dickinson MH. 2003. *J Exp. Biol.* 206:295–302
68. Heide G, Götz KG. 1996. *J. Exp. Biol.* 199:1711–26
69. Wang ZJ, Melfi J Jr. 2015. *The initial observations of fruit fly's flight with its Mb1 motor neuron altered*, Vol. 60, No. 21. Presented at *Annu. Meet. APS Div. Fluid Dyn.*, 68th, Boston (Flies are supplied by Troy Shirangi of Janelia Research Campus.)
70. Bottiger EG, Furshpan E. 1952. *Biol. Bull.* 102:200–11
71. Chabrier J. 1822. *Essai sur le Vol des Insects, et Observations*. Paris: Kessinger
72. Miyan JA, Ewing AW. 1985. *Philos. Trans. R. Soc. Lond. B* 311:271–302
73. Ritter W. 1912. *The flying apparatus of the blow-fly*, Vol. 56, No. 12, Smithson. Misc. Coll., Washington, DC
74. Nachtigall W, Wilson DM. 1967. *J. Exp. Biol.* 47:77–97
75. Dickinson MH, Lighton JRB. 1995. Muscle efficiency and elastic storage in the flight motor of *Drosophila*. *Science* 128:87–89
76. Walker SM, Schwyn DA, Mokso R, Wicklein T, Müller T, et al. 2014. *PLOS Biol.* 12:e1001823
77. Dickinson MH, Tu M. 1997. *Comp. Biochem. Physiol.* 116A(3):223–38
78. Dudley R. 2000. *The Biomechanics of Insect Flight: Form, Function, Evolution*. Princeton, NJ: Princeton Univ. Press
79. Bergou AJ, Xu S, Wang ZJ 2007. *J. Fluid Mech.* 591:321–37
80. Schrödinger E. 1992 (1944). *What Is life? Based on 1943 Lectures at Trinity College, Dublin*. Book version. Cambridge, UK: Cambridge Univ. Press
81. White JG, Southgate E, Thomson JN, Brenner S. 1986. *Philos. Trans. R. Soc. B* 314(1165):1–340

Ⱥ

**Annual Review
of Condensed
Matter Physics**

Volume 7, 2016

Contents

Errata

An online log of corrections to *Annual Review of Condensed Matter Physics* articles may
be found at http://www.annualreviews.org/errata/conmatphys